

Chapter 1

Neutrino Oscillation Phenomenology

Stephen J. Parke

*Theoretical Physics Department, Fermi National Accelerator Laboratory,
P. O. Box 500, Batavia, IL 60510, USA
parke@fnal.gov*

A summary of neutrino oscillation phenomenology is given within the context of the neutrino mixing model (3 active flavors only) for both the disappearance and appearance modes. Extensions of the model to include one or more sterile neutrinos are discussed.

Contents

1.1	Introduction	1
1.2	The ν_e Disappearance Channel	5
1.2.1	Reactor Experiments at the Solar L/E	5
1.2.2	Reactor Experiments at the Atmospheric L/E	6
1.2.3	Solar Neutrinos	7
1.3	The ν_μ Disappearance Channel	10
1.4	The $\nu_\mu \rightarrow \nu_e$ Appearance Channel	11
1.5	Beyond the Neutrino Mixing Model	13
1.6	Summary and Conclusion	16
	References	17

1.1. Introduction

In the Standard Model the neutrinos, $(\nu_e, \nu_\mu, \nu_\tau)$, are massless and interact diagonally in flavor, as follows:

$$\begin{aligned} W^+ &\rightarrow e^+ + \nu_e & W^- &\rightarrow e^- + \bar{\nu}_e & Z &\rightarrow \nu_e + \bar{\nu}_e \\ W^+ &\rightarrow \mu^+ + \nu_\mu & W^- &\rightarrow \mu^- + \bar{\nu}_\mu & Z &\rightarrow \nu_\mu + \bar{\nu}_\mu \\ W^+ &\rightarrow \tau^+ + \nu_\tau & W^- &\rightarrow \tau^- + \bar{\nu}_\tau & Z &\rightarrow \nu_\tau + \bar{\nu}_\tau. \end{aligned} \quad (1.1)$$

Since they travel at the speed of light, their character cannot change from production to detection because the mass eigenstates are the same as the

flavor eigenstates. Therefore, in flavor terms, massless neutrinos are relatively uninteresting compared to quarks.

As evidenced by the subsequent chapters of this volume, several experiments have observed neutrino behavior not explained by the massless neutrino described by the Standard Model. The observations of these experiments can most simply be described by introducing the phenomenon of neutrino flavor transitions. Such flavor transitions imply that neutrinos must have mass. Thus, as in the quark sector, there is a mixing matrix relating the flavor states with the mass eigenstates:

$$|\nu_\alpha\rangle = U_{\alpha j}^* |\nu_j\rangle, \quad (1.2)$$

where $\nu_\alpha = (\nu_e, \nu_\mu, \nu_\tau, \dots)$, represent the flavor states and $\nu_j = (\nu_1, \nu_2, \nu_3, \dots)$ represent the mass eigenstates with mass m_j . The mixing matrix $U_{\alpha j}$ is usually called the MNS^a mixing matrix.¹

Neutrino oscillation experiments typically measure the probability of a neutrino produced as flavor ν_α to be detected as flavor ν_β after traveling some distance. If $\alpha = \beta$, this probability is called the survival probability, and for massive neutrinos this probability is given by

$$P(\nu_\alpha \rightarrow \nu_\alpha) = P(\bar{\nu}_\alpha \rightarrow \bar{\nu}_\alpha) = \left| \sum_j U_{\alpha j}^* e^{-im_j^2 L/2E} U_{\alpha j} \right|^2. \quad (1.3)$$

In words, this is the square of the sum of the amplitudes for the α flavor neutrino to produce a m_j mass state, times a propagator factor, times the amplitude for the m_j mass states to produce the α flavor neutrino. Invariance under CPT forces the survival probability for neutrinos and anti-neutrinos to be identical, in vacuum.

Except for the LSND anomaly, the subject of Chapter 7, all neutrino data can be explained by the following neutrino model:

- 3 light ($m_i < 1$ eV) Neutrinos: only 2 independent Δm^2 ($\Delta m_{ij}^2 = m_i^2 - m_j^2$)
- Three active neutrino flavors (no steriles): ν_e, ν_μ, ν_τ
- Unitary Mixing Matrix: 3 angles ($\theta_{12}, \theta_{23}, \theta_{13}$), 1 Dirac phase (δ), 2 Majorana phases (α, β)

^aAlso referred to as the PMNS matrix.

where the MNS mixing matrix relating flavor to mass eigenstates, can be written as

$$U = \begin{pmatrix} c_{13}c_{12} & c_{13}s_{12} & s_{13}e^{-i\delta} \\ -c_{23}s_{12} - s_{13}c_{12}s_{23}e^{+i\delta} & c_{23}c_{12} - s_{13}s_{12}s_{23}e^{+i\delta} & c_{13}s_{23} \\ s_{23}s_{12} - s_{13}c_{12}c_{23}e^{+i\delta} & -s_{23}c_{12} - s_{13}s_{12}c_{23}e^{+i\delta} & c_{13}c_{23} \end{pmatrix} \times \begin{pmatrix} 1 & & \\ & e^{i\alpha} & \\ & & e^{i\beta} \end{pmatrix} \quad (1.4)$$

where $s_{ij} = \sin\theta_{ij}$ and $c_{ij} = \cos\theta_{ij}$. This representation of the mixing matrix can also be written in the factorized form:

$$U = \begin{pmatrix} 1 & & \\ & c_{23} & s_{23} \\ & -s_{23} & c_{23} \end{pmatrix} \begin{pmatrix} c_{13} & s_{13}e^{-i\delta} \\ & 1 \\ -s_{13}e^{i\delta} & c_{13} \end{pmatrix} \begin{pmatrix} c_{12} & s_{12} \\ -s_{12} & c_{12} \\ & & 1 \end{pmatrix} \times \begin{pmatrix} 1 & & \\ & e^{i\alpha} & \\ & & e^{i\beta} \end{pmatrix} \quad (1.5)$$

In this form, the mixing matrix is decomposed into terms that can be associated with different regimes of mixing that have been explored by different classes of experiments. The (23) sector is identified with the atmospheric Δm_{atm}^2 and the (12) sector is identified with the solar Δm_{\odot}^2 . The (13) sector is responsible for ν_e flavor transitions at the atmospheric scale, which are so far unobserved. The Dirac phase, δ , allows for the possibility of CP violation in the appearance modes.

As will be described in this volume, the current best fit values or limits on these parameters are^b

$$\sin^2\theta_{12} = 0.31 \pm 0.03$$

$$\sin^2\theta_{23} = 0.50 \pm 0.15$$

$$\sin^2\theta_{13} < 0.04$$

$$0 \leq \delta < 2\pi$$

and the mass splittings are approximately:

$$|\Delta m_{32}^2| = 2.7 \pm 0.4 \times 10^{-3} \text{eV}^2 \quad \text{and} \quad \Delta m_{21}^2 = +8.0 \pm 0.4 \times 10^{-5} \text{eV}^2.$$

^bSome experiments report their results in terms of $\sin^2(2\theta)$, others in terms of $\tan^2\theta$. However, $\sin^2\theta$ is used here, since each of the three $\sin^2\theta$'s approximately corresponds to the fraction of a certain flavor in one of the mass eigenstates as follows: $\sin^2\theta_{13} = |U_{e3}|^2 \ll 1$, $\sin^2\theta_{23} \approx |U_{\mu 3}|^2$ and $\sin^2\theta_{12} \approx |U_{e2}|^2$.

Oscillation experiments are only sensitive to the differences in masses of the neutrinos. The mass of the lightest neutrino is unknown, but the heaviest one should be lighter than about 1 eV. These mixing angles and mass splittings are summarized in Fig. 1.1, which also shows the dependence of the flavor fractions on the CP violating Dirac phase, δ . Since the masses of the neutrinos are as yet unknown, there are two possible arrangements of the mass differences that are consistent with the oscillation experiments. These are called the “Normal Hierarchy” and the “Inverted Hierarchy”. The Majorana phases, α and β are unobservable in oscillations since oscillations depend on $U_{\alpha i}^* U_{\beta i}$, but they have observable, CP conserving effects, in neutrinoless double beta decay. If the neutrinos are not Majorana particles, but instead are Dirac particles, then neutrinoless double beta decay will not be observed, and the Majorana phases in the MNS matrix are unobservable and can be set to zero.

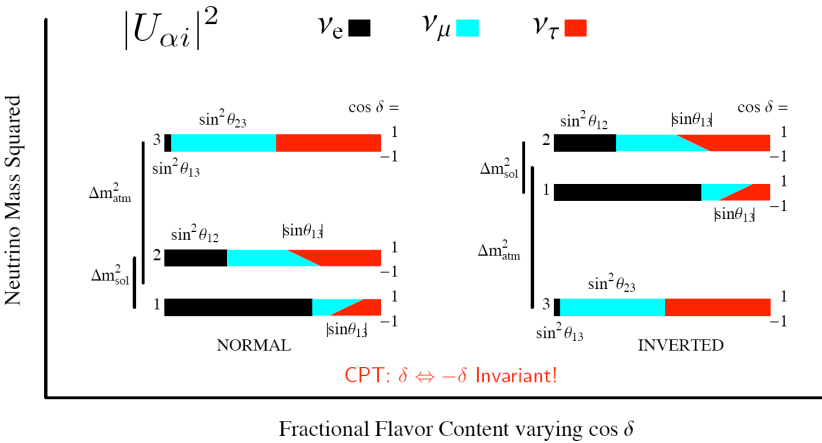


Fig. 1.1. Flavor content of the three neutrino mass eigenstates showing the dependence on the cosine of the CP violating phase, δ . If CPT is conserved, the flavor content must be the same for neutrinos and anti-neutrinos. This figure was adapted from Reference 3.

The unresolved questions within this model that can be addressed in oscillation experiments are

- What is the size of $|U_{e3}|^2$? i.e. $\sin^2 \theta_{13} = ?$
 - Hierarchy: Is $m_3^2 >$ OR $< m_1^2$? i.e. what is the sign of Δm_{31}^2 ?
 - Is there CP violation? i.e. $\sin \delta \neq 0$?
 - Is $|U_{\mu 3}|^2 = |U_{\tau 3}|^2$? i.e. $\sin^2 \theta_{23} = \frac{1}{2}$?
- If not, is $|U_{\mu 3}|^2 >$ or $< |U_{\tau 3}|^2$? i.e. $\sin^2 \theta_{23} >$ or $< \frac{1}{2}$?

Other important questions include

- What is the mass of the lightest neutrino?
- Are Neutrinos Majorana or Dirac?
- Are there more than three neutrinos? Are there sterile neutrinos?
- Do exotic neutrinos interactions exist?

Neutrino oscillation experiments can not answer the first two questions, though they may yet shed light on the final two.

The phenomenology of neutrino oscillations can simplify considerably depending on the values of the parameters involved or on the value of the ratio L/E , the distance traveled divided by the neutrino energy, associated with a given experiment. The following sections discuss specific channels studied by different experiments, the parameters to which they are sensitive, and the approximations that hold in each case.

1.2. The ν_e Disappearance Channel

In the three flavor neutrino model the ν_e survival probability can be written as

$$\begin{aligned}
 P(\nu_e \rightarrow \nu_e) = & 1 - 4|U_{e3}|^2|U_{e1}|^2 \sin^2 \Delta_{31} \\
 & - 4|U_{e3}|^2|U_{e2}|^2 \sin^2 \Delta_{32} \\
 & - 4|U_{e2}|^2|U_{e1}|^2 \sin^2 \Delta_{21}
 \end{aligned} \tag{1.6}$$

where the kinematic phase is given by:

$$\Delta_{jk} \equiv \frac{\Delta m_{jk}^2 L}{4\hbar c E} = 1.2669 \dots \left(\frac{\Delta m_{jk}^2}{eV^2} \right) \left(\frac{L}{km} \right) \left(\frac{GeV}{E} \right) \tag{1.7}$$

and the unitarity properties of the MNS matrix have been used. The survival probability given in Equation 1.6 is plotted as a function of L/E in Figure 1.2.

1.2.1. Reactor Experiments at the Solar L/E

For experiments at the solar L/E (around 15 km/MeV) without the resolution to resolve the atmospheric oscillations on top of the dominant solar oscillation, such as KamLAND⁵ (See Chapter 4), Eq. 1.6 can be written as

$$P(\bar{\nu}_e \rightarrow \bar{\nu}_e) = c_{13}^4 (1 - \sin^2 2\theta_{12} \sin^2 \Delta_{21}) + s_{13}^4. \tag{1.8}$$

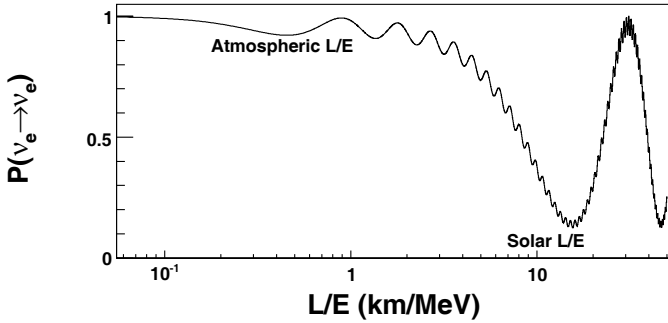


Fig. 1.2. The ν_e survival probability as a function of L/E for the oscillation parameters given in Section 1.1 and $\sin^2 \theta_{13} = 0.02$.

Since s_{13}^4 is known to be very small, $< 10^{-3}$, the only effect of non-zero θ_{13} is a multiplicative reduction of the survival probability. To measure this overall reduction requires precise knowledge of the neutrino flux from the reactor(s). However, the solar parameters and in particular Δm_{21}^2 can be measured with high precision in such an experiment.

1.2.2. Reactor Experiments at the Atmospheric L/E

For experiments at the atmospheric L/E (around 0.5 km/MeV), such as CHOOZ,⁶ Palo Verde,⁷ Double-Chooz⁸ and Daya Bay (See Chapters 12 and 13), the survival probability, Eq. 1.6, can be written as

$$P(\bar{\nu}_e \rightarrow \bar{\nu}_e) = 1 - \sin^2 2\theta_{13} \sin^2 \Delta_{ee} + \mathcal{O}(\Delta_{21}^2) \quad (1.9)$$

where $\Delta_{ee} = \Delta m_{ee}^2 L/4E$, and Δm_{ee}^2 is the effective atmospheric Δm^2 for the ν_e oscillation channel,⁹ given by

$$\Delta m_{ee}^2 \equiv c_{12}^2 |\Delta m_{31}^2| + s_{12}^2 |\Delta m_{32}^2|. \quad (1.10)$$

That is, the electron flavor weighted average of Δm_{31}^2 and Δm_{32}^2 . The experiments Double Chooz and Daya Bay are designed to measure or put a limit on the size of $\sin^2 \theta_{13}$ significantly below the current limit of

$$\sin^2 \theta_{13} < 0.04 \quad (1.11)$$

at the best fit value for the atmospheric Δm^2 .

1.2.3. Solar Neutrinos

Solar neutrinos are somewhat more complicated because of the matter effects that the neutrinos experience from the production region until they exit the sun. As the neutrino propagates in matter, the electron neutrino plays a special role due to the forward scattering of the electron neutrino on the electrons in the matter coming from W-boson exchange, i.e. the charged current interaction^c. This additional contribution to the Hamiltonian from $\nu_e + e$ scattering is $-\sqrt{2}G_F N_e$, which appears only for the electron neutrino. For $\bar{\nu}_e + e$ scattering the sign is flipped. G_F is the Fermi constant and N_e is the number density of electrons in matter. This implies that the matter mass eigenstates are different than the vacuum mass eigenstates and that the Δm^2 and mixing angle, θ , in matter are related to their vacuum values as follows:

$$\begin{aligned}\Delta m_N^2 \cos 2\theta_N &= \Delta m_0^2 \cos 2\theta_0 - 2\sqrt{2}G_F N_e E_\nu \\ \Delta m_N^2 \sin 2\theta_N &= \Delta m_0^2 \sin 2\theta_0.\end{aligned}\quad (1.12)$$

The subscript on Δm^2 and θ denotes the value of the number density of electrons. For large values of the number density of electrons, the mixing angle in matter, θ_N , approaches $\pi/2$. Thus, the higher neutrino mass state becomes nearly completely ν_e . The minimum value of Δm_N^2 occurs when $\Delta m_0^2 \cos 2\theta_0 = 2\sqrt{2}G_F N_e E_\nu$ and $\theta_N = \pi/4$. This point is known as the Mikheyev-Smirnov resonance.

The matter effect is proportional to the energy of the neutrino. Since the pp (${}^7\text{Be}$) have a mean energy of 0.2 MeV (0.9 MeV), these neutrinos are little affected by the matter and undergo quasi-vacuum oscillations. The ${}^8\text{B}$ neutrinos, on the other hand, have a mean energy of 10 MeV and because of matter effects are produced and exit the sun mainly as a ν_2 mass eigenstate and therefore do not undergo vacuum oscillations.

The kinematic phase for solar neutrinos is

$$\Delta_\odot = \frac{\Delta m_\odot^2 L}{4E} = 10^{7\pm 1}.\quad (1.13)$$

where $\Delta m_\odot^2 = \Delta m_{21}^2$. Therefore, the solar neutrinos are “effectively incoherent” when they reach the earth. Hence the ν_e survival probability is given by

$$\langle P(\nu_e \rightarrow \nu_e) \rangle = f_1 \cos^2 \theta_\odot + f_2 \sin^2 \theta_\odot \quad (1.14)$$

$$\text{where } f_1 + f_2 = 1 \quad \text{and} \quad \cos^2 \theta_\odot + \sin^2 \theta_\odot = 1,$$

^cInteractions via Z-bosons are the same for all flavors and therefore effect all neutrinos equally.

where f_1 and f_2 are the fraction of neutrinos that are ν_1 and ν_2 respectively. The pp and ${}^7\text{Be}$ solar neutrinos behave essentially as in vacuum^d and therefore $f_1 \approx \cos^2 \theta_\odot = 0.69$ and $f_2 \approx \sin^2 \theta_\odot = 0.31$, whereas the mass eigenstate fraction for the ${}^8\text{B}$ are substantially different, $f_2 \approx 0.9$ due to Mikheyev-Smirnov-Wolfenstein¹⁰ matter effects (see Fig. 1.3).

In a two neutrino analysis, the *day-time* charged current to neutral current ratio (CC/NC) of SNO (See Chapter 3), which is equivalent to the day-time average ν_e survival probability, $\langle P_{ee} \rangle = P(\nu_e \rightarrow \nu_e)$, is given by

$$\left. \frac{\text{CC}}{\text{NC}} \right|_{\text{day}} = \langle P_{ee} \rangle = \sin^2 \theta_\odot + f_1 \cos 2\theta_\odot, \quad (1.15)$$

where f_1 and $f_2 = 1 - f_1$ are understood to be the ν_1 and ν_2 fractions, respectively, averaged over the ${}^8\text{B}$ neutrino energy spectrum weighted with the charged current cross section. Therefore, the ν_1 fraction (or how much f_2 differs from 100%) is given by

$$f_1 = \frac{\left(\left. \frac{\text{CC}}{\text{NC}} \right|_{\text{day}} - \sin^2 \theta_\odot \right)}{\cos 2\theta_\odot} = \frac{(0.347 - 0.311)}{0.378} \approx 10 \%, \quad (1.16)$$

where the central values of the recent SNO analysis¹¹ have been used.

For solar neutrinos the matter effects on Δm^2 and θ are shown in Fig. 1.3. As the electron number density^e times energy of the neutrinos gets larger, the mixing angle approaches $\pi/2$ and the Δm^2 approaches $2\sqrt{2}G_F N_e E_\nu$. Therefore, a solar ν_e born in an environment with high $2\sqrt{2}G_F N_e E_\nu$ is approximately born as a ν_2 matter mass eigenstate.

Using the analytical analysis of the MSW effect given in Reference 12, the mass eigenstate fractions are given by

$$f_2 = 1 - f_1 = \langle \sin^2 \theta_\odot^N + P_x \cos 2\theta_\odot^N \rangle_{s_B}, \quad (1.17)$$

where θ_\odot^N is the mixing angle defined at the ν_e production point and P_x is the probability of the neutrino to jump from one mass eigenstate to the other during the Mikheyev-Smirnov (MS) resonance crossing. In the large mixing angle region P_x is zero to high precision. The average $\langle \dots \rangle_{s_B}$ is over the electron density of the ${}^8\text{B}$ ν_e production region in the center of the Sun predicted by the Standard Solar Model and the energy spectrum

^dIn vacuum, a ν_e has a ν_1 fraction equal to $\cos^2 \theta_\odot$ and a ν_2 fraction equal to $\sin^2 \theta_\odot$. Whereas the probability of finding a ν_e in a ν_1 is $\cos^2 \theta_\odot$, for a ν_2 , the ν_e fraction is $\sin^2 \theta_\odot$.

^e $N_e = \rho Y_e / M_n$ where Y_e is the electron fraction, ρ is the density and M_n is the nucleon mass.

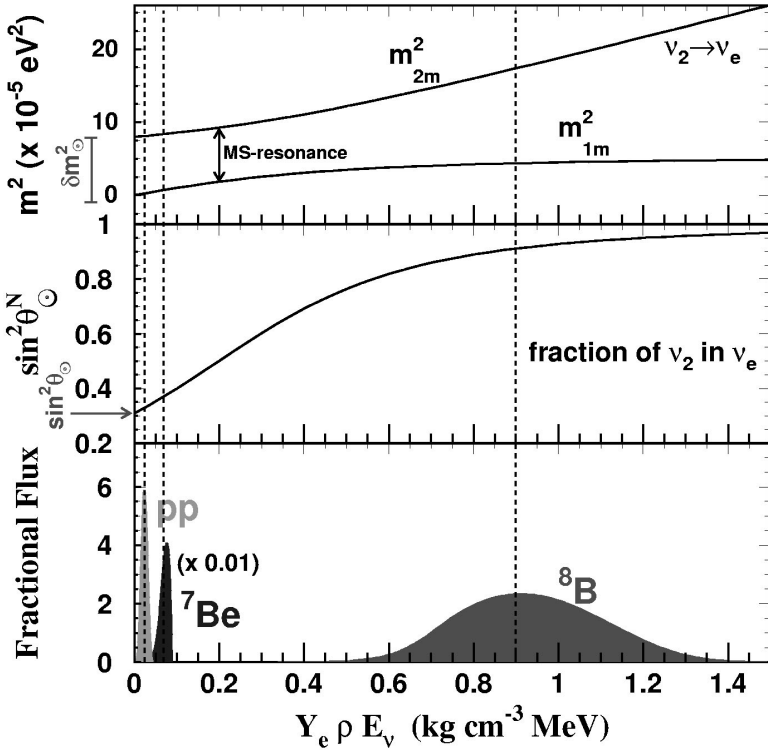


Fig. 1.3. The mass spectrum (top panel), the fraction of ν_2 's produced, $\sin^2 \theta_{\odot}^N$, (middle panel) and the fractional flux (bottom panel) versus the product of the electron fraction, Y_e , the matter density, ρ , and the neutrino energy, E_ν , for the best fit values $\Delta m_{\odot}^2 = 8.0 \times 10^{-5} \text{eV}^2$ and $\sin^2 \theta_{\odot} = 0.310$. The vertical dashed lines give the value of $Y_e \rho E_\nu$ which reproduces the average ν_2 fractions, 91, 37 and 33% for ${}^8\text{B}$, ${}^7\text{Be}$ and pp respectively. This value of $Y_e \rho E_\nu = 0.89 \text{kg cm}^{-3} \text{MeV}$, for the ${}^8\text{B}$ neutrinos, gives a production mixing angle equal to 73° and a production $\Delta m_N^2 = 13 \times 10^{-5} \text{eV}^2$. The matter potential, A , is related to density factor, $Y_e \rho E_\nu$, by $A \equiv 2\sqrt{2}G_F(Y_e \rho/M_n)E_\nu = 15.3 \times 10^{-5} \text{eV}^2 (Y_e \rho E_\nu/\text{kg cm}^{-3} \text{MeV})$. Reproduced from Reference 13.

of ${}^8\text{B}$ neutrinos weighted with SNO's charged current cross section. Thus, the ${}^8\text{B}$ energy weighted average fraction of ν_2 's observed by SNO is¹³

$$\begin{aligned}
 f_2 &= \langle \sin^2 \theta_{\odot}^N \rangle_{8\text{B}} = \frac{1}{2} + \frac{1}{2} \left\langle \frac{(A - \Delta m_{\odot}^2 \cos 2\theta_{\odot})}{\sqrt{(\Delta m_{\odot}^2 \cos 2\theta_{\odot} - A)^2 + (\Delta m_{\odot}^2 \sin 2\theta_{\odot})^2}} \right\rangle_{8\text{B}} \\
 &= 91 \pm 2\% \quad \text{at the 95\% CL,} \tag{1.18}
 \end{aligned}$$

where $A = 2\sqrt{2}G_F(Y_e\rho/M_n)E\nu$. Hence, the ^8B solar neutrinos are the purest mass eigenstate neutrino beam known so far, and Super-K's¹⁴, famous picture of the sun taken with neutrinos is more than 80% ν_2 !

1.3. The ν_μ Disappearance Channel

In vacuum, the ν_μ survival probability is given by

$$\begin{aligned}
 P(\nu_\mu \rightarrow \nu_\mu) = & 1 - 4|U_{\mu 3}|^2|U_{\mu 1}|^2 \sin^2 \Delta_{31} \\
 & - 4|U_{\mu 3}|^2|U_{\mu 2}|^2 \sin^2 \Delta_{32} \\
 & - 4|U_{\mu 2}|^2|U_{\mu 1}|^2 \sin^2 \Delta_{21}.
 \end{aligned} \tag{1.19}$$

The ν_μ survival probability is plotted as a function of E at a fixed L in Figure 1.4.

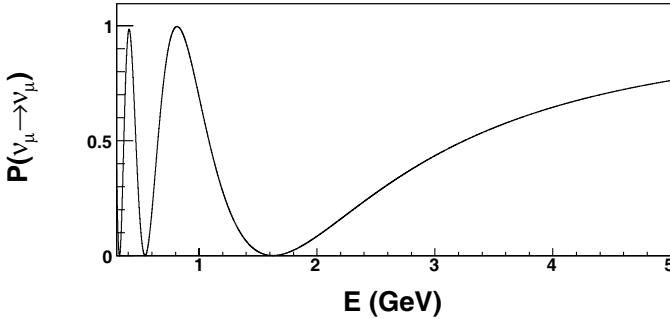


Fig. 1.4. The ν_μ survival probability as a function of E for the oscillation parameters given in Section 1.1 and $L = 735$ km.

For experiments at the atmospheric L/E (around 500 km/GeV), such as K2K,¹⁵ MINOS,¹⁶ T2K¹⁷ and NO ν A¹⁸ (See Chapters 5, 6, 10, and 11) in $\nu_\mu \rightarrow \nu_\mu$ mode, Eq. 1.19, can be written as

$$P(\nu_\mu \rightarrow \nu_\mu) = 1 - 4|U_{\mu 3}|^2(1 - |U_{\mu 3}|^2) \sin^2 \Delta_{\mu\mu} + \mathcal{O}(\Delta_{21}^2) \tag{1.20}$$

where $|U_{\mu 3}|^2 = c_{13}^2 s_{23}^2$ and $\Delta_{\mu\mu} = \Delta m_{\mu\mu}^2 L/4E$. $\Delta m_{\mu\mu}^2$ is the effective

atmospheric Δm^2 for the ν_μ disappearance channel^f given by

$$\Delta m_{\mu\mu}^2 \equiv \frac{|U_{\mu 1}|^2 |\Delta m_{31}^2| + |U_{\mu 2}|^2 |\Delta m_{32}^2|}{(|U_{\mu 1}|^2 + |U_{\mu 2}|^2)}, \quad (1.21)$$

i.e. the muon flavor weighted average of Δm_{31}^2 and Δm_{32}^2 . In the limit that $\theta_{13} \rightarrow 0$

$$4|U_{\mu 3}|^2(1 - |U_{\mu 3}|^2) = \sin^2 2\theta_{23} \quad (1.22)$$

$$\text{and } \Delta m_{\mu\mu}^2 = s_{12}^2 |\Delta m_{31}^2| + c_{12}^2 |\Delta m_{32}^2|. \quad (1.23)$$

The difference between $\Delta m_{\mu\mu}^2$ and $|\Delta m_{32}^2|$ is given by $\pm s_{12}^2 \Delta m_{21}^2$ which is approximately a 1% shift whose sign depends on the hierarchy. This form of the oscillation probability is used by Super-K (See Chapter 2) in their two flavor analysis of atmospheric neutrinos.

1.4. The $\nu_\mu \rightarrow \nu_e$ Appearance Channel

The most likely genuine three flavor effects to be first observed are long baseline $\nu_\mu \rightarrow \nu_e$ or one of its CP and T conjugate processes. That is, in one of following transitions:

$$\begin{array}{ccccc} & & \text{CP} & & \\ & & \iff & & \\ & \nu_\mu \rightarrow \nu_e & & \bar{\nu}_\mu \rightarrow \bar{\nu}_e & \\ & & \text{T} & & \text{T} \\ & \updownarrow & & \updownarrow & \\ & \nu_e \rightarrow \nu_\mu & \iff & \bar{\nu}_e \rightarrow \bar{\nu}_\mu & \\ & & \text{CP} & & \end{array}$$

Processes across the diagonal are related by CPT. The first row will be explored in very powerful conventional beams, called Superbeams. Such beams are accessible with extensions of currently available technologies. The second row could be explored using more exotic techniques involving a Neutrino Factory or a Beta Beam, a pure beam of ν_e produced via the beta decay of accelerated radioactive ions.

^fThe difference between the two effective atmospheric Δm^2 is small and depends on the hierarchy. $\Delta m_{ee}^2 - \Delta m_{\mu\mu}^2 = \pm \Delta m_{21}^2 (\cos 2\theta_{12} - \cos \delta \sin \theta_{13} \sin 2\theta_{12} \tan \theta_{23})$ where the + (-) is for the normal (inverted) hierarchies.⁹

In vacuum, the probability for $\nu_\mu \rightarrow \nu_e$ is derived like so:¹⁹

$$\begin{aligned} P(\nu_\mu \rightarrow \nu_e) &= |U_{\mu 1}^* e^{-im_1^2 L/2E} U_{e1} + U_{\mu 2}^* e^{-im_2^2 L/2E} U_{e2} + U_{\mu 3}^* e^{-im_3^2 L/2E} U_{e3}|^2 \\ &= |2U_{\mu 3}^* U_{e3} \sin \Delta_{31} e^{-i\Delta_{32}} + 2U_{\mu 2}^* U_{e2} \sin \Delta_{21}|^2 \\ &\approx |\sqrt{P_{atm}} e^{-i(\Delta_{32} + \delta)} + \sqrt{P_{sol}}|^2 \end{aligned} \quad (1.24)$$

where the unitarity of the MNS matrix has been used, $U_{\mu 1}^* U_{e1} + U_{\mu 2}^* U_{e2} + U_{\mu 3}^* U_{e3} = 0$, and $\sqrt{P_{atm}} = \sin \theta_{23} \sin 2\theta_{13} \sin \Delta_{31}$ and $\sqrt{P_{sol}} \approx \cos \theta_{23} \sin 2\theta_{12} \sin \Delta_{21}$. For anti-neutrinos δ must be replaced with $-\delta$ and the interference term changes:

$$2\sqrt{P_{atm}} \sqrt{P_{sol}} \cos(\Delta_{32} + \delta) \Rightarrow 2\sqrt{P_{atm}} \sqrt{P_{sol}} \cos(\Delta_{32} - \delta).$$

Expanding $\cos(\Delta_{32} \pm \delta)$, one has a CP conserving part,

$$2\sqrt{P_{atm}} \sqrt{P_{sol}} \cos \Delta_{32} \cos \delta \quad (1.25)$$

and the CP violating part,

$$\mp 2\sqrt{P_{atm}} \sqrt{P_{sol}} \sin \Delta_{32} \sin \delta, \quad (1.26)$$

where - (+) sign is for neutrino (anti-neutrino). This allows for the possibility that CP violation could be observed in the neutrino sector since it allows for $P(\nu_\mu \rightarrow \nu_e) \neq P(\bar{\nu}_\mu \rightarrow \bar{\nu}_e)$.

In matter, $\sqrt{P_{atm}}$ and $\sqrt{P_{sol}}$ are modified as follows:

$$\begin{aligned} \sqrt{P_{atm}} &\Rightarrow \sin \theta_{23} \sin 2\theta_{13} \frac{\sin(\Delta_{31} - aL)}{(\Delta_{31} - aL)} \Delta_{31} \\ \sqrt{P_{sol}} &\Rightarrow \cos \theta_{23} \sin 2\theta_{12} \frac{\sin(aL)}{(aL)} \Delta_{21}, \end{aligned} \quad (1.27)$$

where $a = \pm G_F N_e / \sqrt{2} \approx (4000 \text{ km})^{-1}$, and the sign is positive for neutrinos and negative for anti-neutrinos. This change follows since in both the (31) and (21) sectors, the product $\{\Delta m^2 \sin 2\theta\}$ is approximately independent of matter effects. Figure 1.5 shows the ν_e appearance probability as a function of the distance for neutrinos and anti-neutrinos for both mass orderings at an energy appropriate for T2K, $E=0.6 \text{ GeV}$. Fig. 1.6 shows the ν_e appearance probability as a function of the neutrino energy at a distance appropriate for NO ν A, $L=810 \text{ km}$. In Figs. 1.7 and 1.8 the correlation between the ν_e appearance oscillation probabilities for neutrinos and antineutrinos are shown for both T2K, and NO ν A. It is possible that these two experiments will determine the mass ordering (normal or inverted hierarchy, see Fig. 1.1), and observe CP violation in the neutrino sector.

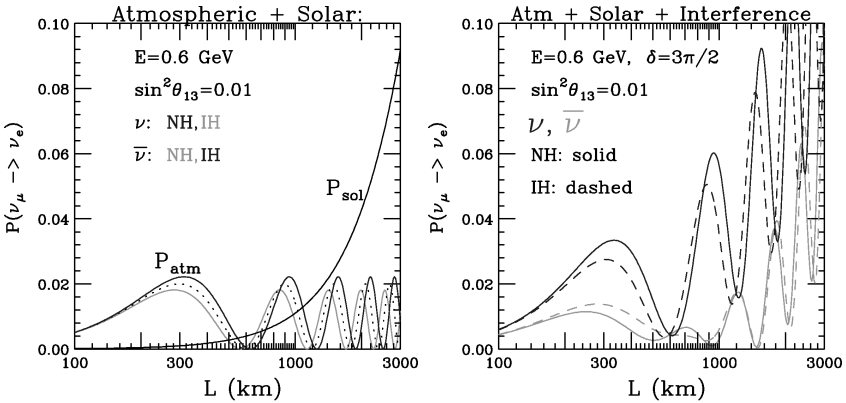


Fig. 1.5. The left panel shows the atmospheric and solar components of the ν_e appearance probability for a neutrino energy of 0.6 GeV for both neutrinos and anti-neutrinos and both mass orderings as a function of the baseline. The dotted P_{atm} curve is the vacuum atmospheric appearance probability. P_{sol} is independent of the hierarchy and the same for neutrinos and anti-neutrinos. The T2K experiment will be performed at approximately this energy at a distance of 295 km and, if constructed, T2KK will be around 1000 km. The right panel shows the full appearance probability including the interference term for $\delta = 3\pi/2$. The appearance probabilities for $\delta = \pi/2$ can be obtained from these, by interchanging normal and inverted as well as neutrinos and anti-neutrinos.

1.5. Beyond the Neutrino Mixing Model

Except for the LSND anomaly²⁰ (See Chapter 7), all neutrino flavor transitions observed so far can be explained using three massive neutrinos that are orthogonal mixtures of the three neutrinos of given flavor. The LSND anomaly is the observation of $\bar{\nu}_\mu \rightarrow \bar{\nu}_e$ at an L/E of order 500 m/GeV with a transition probability of 0.2%. This suggested the possibility of one or more additional neutrinos which have a squared mass splitting from the active neutrinos of order 1 eV^2 . These additional light neutrinos cannot have $SU(2) \times U(1)$ quantum numbers, otherwise their effects would have been observed in other processes, e.g. the decay of Z-boson. Hence, they are called sterile neutrinos. One additional sterile neutrino is marginally compatible with all existing data in the 3+1 scenario^g. The strongest constraints on this model come from ν_e and ν_μ disappearance experiments. The disappearance of ν_e at the LSND L/E depends on the fraction, $|U_{e4}|^2$, of ν_e in the additional 4th-neutrino and similarly for ν_μ . The non-observation

^gIn the 3+1 model the additional neutrino is split from the other neutrinos by order of 1 eV^2 .

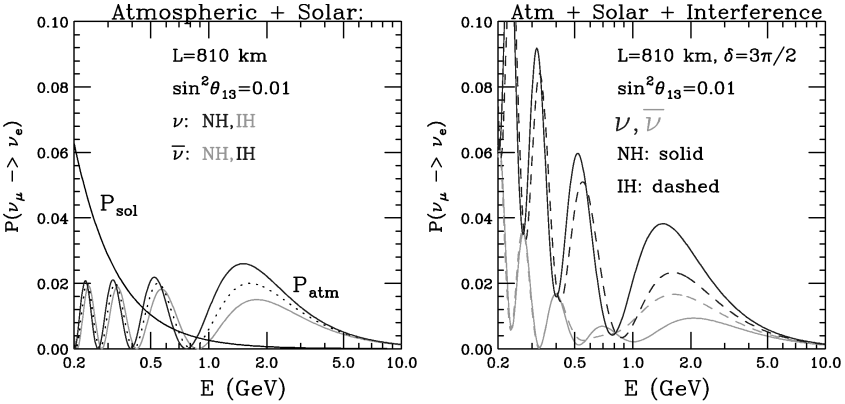


Fig. 1.6. The left panel shows the atmospheric and solar components of the ν_e appearance probability at a distance of 810 km for both neutrinos and anti-neutrinos and both mass orderings as a function of the neutrino energy. The dotted P_{atm} curve is the vacuum atmospheric appearance probability. P_{sol} is independent of the hierarchy and the same for neutrinos and anti-neutrinos. The NO ν A experiment will be performed at this distance with an energy centered at 2 GeV. If an experiment is mounted at the second oscillation maximum at this distance the energy would be approximately 0.6 GeV. The right panel shows the full appearance probability including the interference term for $\delta = 3\pi/2$. The appearance probabilities for $\delta = \pi/2$ can be obtained from these, by interchanging normal and inverted as well as neutrinos for anti-neutrinos.

of disappearance of both ν_e and ν_μ , implies that both $|U_{e4}|^2$ and $|U_{\mu4}|^2$ are small. In this 3+1 model, the LSND appearance of $\bar{\nu}_e$ from $\bar{\nu}_\mu$ depends on the product of these two small quantities, $|U_{e4}|^2|U_{\mu4}|^2$. Thus, moderate limits on the disappearance modes can severely constrain the appearance mode. In a full analysis of both the disappearance and appearance channels, only a few small atolls are not excluded at high confidence level in the $\{\Delta m^2, \sin^2 2\theta\}_{LSND}$ plane. The 2+2 scenario^h is strongly disfavored, since both the solar and atmospheric oscillations are primarily due to active neutrino oscillations. In this model one or both of these phenomena would have to have a substantial sterile neutrino component.

What about the possibility of more than one sterile neutrino? With two or more additional neutrinos the parameters can be chosen so as to be compatible with all existing data, even with the recent non-observation by MiniBooNE²¹ (See Chapter 8) of $\nu_\mu \rightarrow \nu_e$ at the same L/E and sensitivity as LSND.²² This can occur because of the possibility of CP violation at

^hIn the 2+2 model the solar neutrino pair is split from the atmospheric neutrino pair by order of 1eV^2 .

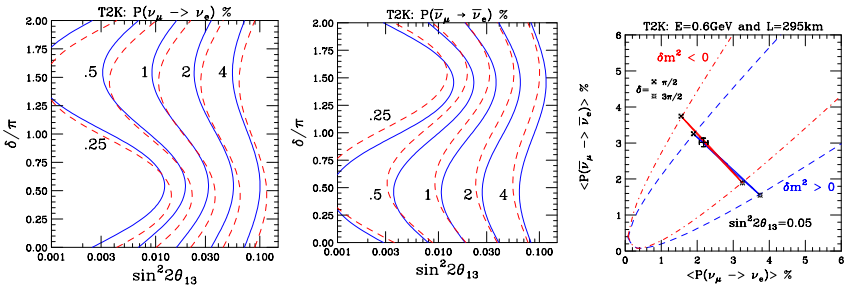


Fig. 1.7. The left and middle panels are the iso-probability contours for T2K as a % for the neutrino (left) and anti-neutrino (middle) channels. The solid (blue) line is for the normal hierarchy whereas the dashed (red) line is for the inverted hierarchy. The right panel is the bi-probability plot showing the correlation between the two probabilities and is reproduced from Reference 4. The matter effect is small but non-negligible for T2K.

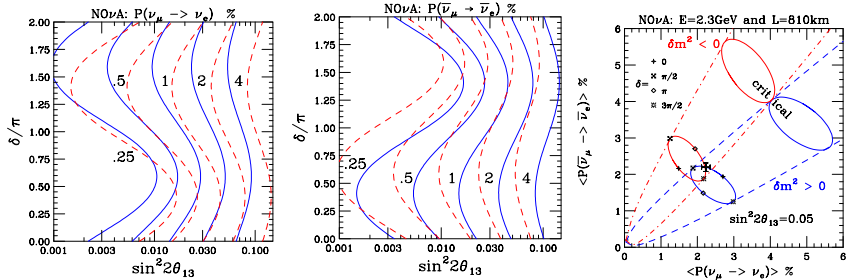


Fig. 1.8. The left and middle panels are the iso-probability contours for NOνA as a % for the neutrino (left) and anti-neutrino (middle) channels. The solid (blue) line is for the normal hierarchy whereas the dashed (red) line is for the inverted hierarchy. The right panel is the bi-probability plot showing the correlation between the two probabilities and is reproduced from Reference 4. The matter effects, and hence the separation between the hierarchies, is 3 times larger for NOνA than T2K primarily due to the fact NOνA has three times the baseline as T2K. The difference in the matter effect between T2K and NOνA can be used to untangle CP violation and the mass hierarchy.

the LSND L/E in models with two or more additional neutrinos. Let us consider the 3+2 model in some detail. If we label the masses of the two additional neutrinos m_4 and m_5 then following Eq. 1.24 gives

$$\begin{aligned}
 P(\nu_\mu \rightarrow \nu_e) &= |2U_{\mu 5}^* U_{e 5} \sin \Delta_{51} e^{-i\Delta_{54}} + 2U_{\mu 4}^* U_{e 4} \sin \Delta_{41}|^2 \\
 &= 4|U_{\mu 5}|^2 |U_{e 5}|^2 \sin^2 \Delta_{51} + 4|U_{\mu 4}|^2 |U_{e 4}|^2 \sin^2 \Delta_{41} \\
 &\quad + 8|U_{\mu 5}| |U_{e 5}| |U_{\mu 4}| |U_{e 4}| \\
 &\quad \times \sin \Delta_{51} \sin \Delta_{41} \cos(\Delta_{54} + \delta_{54})
 \end{aligned}
 \tag{1.28}$$

where $\delta_{54} = \pm \arg(U_{\mu 5}^* U_{e 5} U_{\mu 4} U_{e 4}^*)$. The positive sign is for $\nu_\mu \rightarrow \nu_e$ whereas the negative sign is for $\bar{\nu}_\mu \rightarrow \bar{\nu}_e$. At the LSND L/E the difference between the masses, m_1 , m_2 and m_3 is too small to be relevant, so m_1 has been used as the common mass of these neutrinos, i.e. $\Delta_{51} \approx \Delta_{52} \approx \Delta_{53}$ and $\Delta_{41} \approx \Delta_{42} \approx \Delta_{43}$. The last term of Eq. 1.28 is the interference term between the two amplitudes which can be constructive for $\bar{\nu}_\mu \rightarrow \bar{\nu}_e$ and destructive for $\nu_\mu \rightarrow \nu_e$, allowing for the possibility that

$$P(\bar{\nu}_\mu \rightarrow \bar{\nu}_e) > P(\nu_\mu \rightarrow \nu_e). \quad (1.29)$$

This is a possible explanation of why LSND saw a signal in anti-neutrinos, whereas MiniBooNE does not see a signal in neutrinos at approximately the same sensitivity. The ν_e and ν_μ survival probabilities are given by

$$\begin{aligned} P(\nu_\alpha \rightarrow \nu_\alpha) &= P(\bar{\nu}_\alpha \rightarrow \bar{\nu}_\alpha) \\ &\approx 1 - 4|U_{\alpha 5}|^2 \sin^2 \Delta_{51} - 4|U_{\alpha 4}|^2 \sin^2 \Delta_{41} \\ &\quad + \mathcal{O}((|U_{\alpha 4}|^2 + |U_{\alpha 5}|^2)^2) \end{aligned} \quad (1.30)$$

where $\nu_\alpha = \nu_e$ or ν_μ . The spreading of the limit on the survival probabilities between two distinct Δm^2 , Δm_{41}^2 and Δm_{51}^2 , reduces the severity of the constraints on the appearance modes compared to the 3+1 models. An improvement on the limit of both disappearance modes by a factor of $\sqrt{2}$ would improve the constraint on the appearance mode by a factor of 2 for all values of the CP violating phase δ_{54} .

1.6. Summary and Conclusion

A summary of neutrino oscillation phenomenology has been presented. The oscillation probabilities in the disappearance channels for ν_e and ν_μ flavors have been presented with the relevant approximations for the experiments that will be discussed later in this volume. The appearance probability for $\nu_\mu \rightarrow \nu_e$ and $\bar{\nu}_\mu \rightarrow \bar{\nu}_e$ has been discussed in some detail with particular attention to the unresolved questions associated with the neutrino mass hierarchy and CP violation. This channel is the most likely one to provide the first observation of genuine three flavor effects.

Beyond the 3 flavor mixing model, the addition of one or more sterile neutrinos has been discussed. In these models, there are additional L/E 's for which oscillation phenomena can potentially be observed. If there is more than one additional neutrino, CP violating effects can be important.

Acknowledgments

I would like to thank the editors of this review for their critical reading of this article and their suggestions for improvements. Fermilab is operated by URA under DOE contract DE-AC02-76CH03000.

References

1. Z. Maki, M. Nakagawa and S. Sakata, Prog. Theor. Phys. **28**, 870 (1962).
2. W. M. Yao *et al.* [Particle Data Group], J. Phys. G **33**, 1 (2006).
3. O. Mena and S. J. Parke, Phys. Rev. D **69**, 117301 (2004) [arXiv:hep-ph/0312131].
4. O. Mena and S. J. Parke, Phys. Rev. D **70**, 093011 (2004) [arXiv:hep-ph/0408070].
5. K. Eguchi *et al.* [KamLAND Collaboration], Phys. Rev. Lett. **90**, 021802 (2003). T. Araki *et al.* [KamLAND Collaboration], Phys. Rev. Lett. **94**, 081801 (2005).
6. M. Apollonio *et al.* [CHOOZ Collaboration], Phys. Lett. B **466**, 415 (1999).
7. F. Boehm *et al.*, Phys. Rev. D **64**, 112001 (2001) [arXiv:hep-ex/0107009].
8. F. Ardellier *et al.* [Double Chooz Collaboration], arXiv:hep-ex/0606025.
9. H. Nunokawa, S. J. Parke and R. Zukanovich Funchal, Phys. Rev. D **72**, 013009 (2005) [arXiv:hep-ph/0503283]. H. Minakata, H. Nunokawa, S. J. Parke and R. Zukanovich Funchal, Phys. Rev. D **74**, 053008 (2006) [arXiv:hep-ph/0607284].
10. L. Wolfenstein, Phys. Rev. D **17**, 2369 (1978) and Neutrino 1978, pg C3-C6 edited by E. C. Fowler. S. P. Mikheyev and A. Yu. Smirnov, Yad. Fiz. **42**, 1441 (1985) [Sov. J. Nucl. Phys. **42**, 913 (1985)]; Nuovo Cim. C **9**, 17 (1986).
11. B. Aharmim *et al.* [SNO Collaboration], arXiv:nucl-ex/0502021. Also in this volume.
12. S. J. Parke, Phys. Rev. Lett. **57**, 1275 (1986); S. J. Parke and T. P. Walker, Phys. Rev. Lett. **57**, 2322 (1986).
13. H. Nunokawa, S. J. Parke and R. Zukanovich Funchal, Phys. Rev. D **74**, 013006 (2006) [arXiv:hep-ph/0601198].
14. K. S. Hirata *et al.* [KAMIOKANDE-II Collaboration], Phys. Rev. Lett. **65**, 1297 (1990); M. B. Smy *et al.* [Super-Kamiokande Collaboration], Phys. Rev. D **69**, 011104 (2004); J. Hosaka *et al.* [Super-Kamiokande Collaboration], arXiv:hep-ex/0508053.
15. E. Aliu *et al.* [K2K Collaboration], Phys. Rev. Lett. **94**, 081802 (2005) [arXiv:hep-ex/0411038].
16. D. G. Michael *et al.* [MINOS Collaboration], Phys. Rev. Lett. **97**, 191801 (2006) [arXiv:hep-ex/0607088].
17. Y. Itow *et al.*, arXiv:hep-ex/0106019.
18. D. S. Ayres *et al.* [NOvA Collaboration], arXiv:hep-ex/0503053.
19. A. Cervera, A. Donini, M. B. Gavela, J. J. Gomez Cadenas, P. Hernandez, O. Mena and S. Rigolin, Nucl. Phys. B **579**, 17 (2000) [Erratum-ibid. B **593**,

- 731 (2001)] [arXiv:hep-ph/0002108].
20. A. Aguilar *et al.* [LSND Collaboration], Phys. Rev. D **64**, 112007 (2001) [arXiv:hep-ex/0104049].
 21. A. A. Aguilar-Arevalo *et al.* [The MiniBooNE Collaboration], arXiv:0704.1500 [hep-ex].
 22. G. Karagiorgi, A. Aguilar-Arevalo, J. M. Conrad, M. H. Shaevitz, K. Whisnant, M. Sorel and V. Barger, Phys. Rev. D **75**, 013011 (2007) [arXiv:hep-ph/0609177].